Kinetics and Catalysis, Vol. 41, No. 2, 2000, pp. 242–254. Translated from Kinetika i Kataliz, Vol. 41, No. 2, 2000, pp. 267–280.

Mechanism of ·OH Formation in the Thermal Decomposition of $(\equiv Si–O)_2Si(C_2H_5)(O–O^{\cdot})$ Radicals

V. A. Radtsig and S. N. Kostritsa

Semenov Institute of Chemical Physics, Russian Academy of Sciences, Moscow, 117977 Russia

Received December 30, 1998

Abstract—ESR and IR spectroscopy and quantum chemical calculations are used to obtain the mechanistic data on the reaction $(\equiv Si–O)_2Si(C_2H_5)(O–O^{\cdot}) \longrightarrow (\equiv Si–O)_2Si\langle^{O}_{CH_2}\rangle CH_2 + {}^{\cdot}OH$. The IR bands are assigned by simulating the vibrational spectra of model low-molecular compounds. Quantum chemical calculations provided the data on the shapes of potential energy surface for the systems under study and transition states. These data are used to interpret the experimental data. The title reaction occurs much more readily in the case of organosilicon peroxy radicals than in the case of their hydrocarbon analogs. Surface silanone groups of silica react with ethylene molecules to form the siloxacyclobutane group.

INTRODUCTION

Peroxy radicals play a key role in the oxidation of organic and organosilicon compounds. However, most experimental data refer to bimolecular processes, such as hydrogen atom abstraction and radical reactions with other molecules and radicals in a system. Monomolecular reactions of peroxy radicals are less studied. The experimental studies of these processes are complicated by the following factors. The reactions of peroxy radicals are usually studied in the gas or condensed phases where monomolecular reactions are usually masked by the bimolecular reactions of radicals with surrounding molecules or with each other. These bimolecular reactions are faster. The matrix-isolation technique enables the stabilization of peroxy radicals, but matrices are thermally unstable. Therefore, these systems cannot be used to study the processes with the activation energies higher than several kilocalories per mole.

Radtsig and co-workers [1–3] proposed earlier the method for obtaining radical fragments grafted on a solid surface (activated silica). The accessibility of sites (defects) to the molecules of a medium enables their chemical modification on purpose and the obtainment of the structures of a desirable chemical nature. Siloxane bonds, which are chemically inert, comprise the closest neighborhood of radical fragments thus obtained. As a result, the radical fragments are matrix-stabilized. The thermal stability of these fragments, which bind chemically to the solid surface, is determined by their reactivity in intramolecular reactions (isomerization and decomposition). The low-molecular radical products of these transformations can be identified. Diamagnetic defects, which are also stabilized on the surface of activated silica, are efficient acceptors of these species (spin traps) [2, 3]. By identifying the structure of paramagnetic complexes formed, we may obtain information on low-molecular radicals, which are formed in thermal or photochemical transformations of the surface-grafted centers. Thus, the use of this technique opens new avenues for obtaining various radical fragments and studying their spectral properties and reactivity.

In this article, we propose a new method for generating silicon-centered peroxy radicals $(\equiv Si–O)_2Si(C_2H_5)(O–O^{\cdot})$ in which $(\equiv Si–O)_2Si$ is a fragment of a solid, involving the surface silicon atom. We report the results of the experimental and theoretical (quantum chemical) study of the intramolecular transformations of these radicals. In the last few years, mechanisms of radical reactions with organosilicon compounds have attracted considerable attention due to their diverse applications, especially in microelectronics and fiber optics. However, to the best of our knowledge, there are no experimental data on the directions and kinetics of the processes of the intramolecular transformations of these radicals.

The structure of surface groups was controlled using spectral (ESR, IR, and optical) methods. A combination of these methods provided the information on paramagnetic and diamagnetic products of transformations. To interpret the experimental data, we used *ab initio* quantum chemical calculations of the model systems.

EXPERIMENTAL

All experiments were carried out with highly-dispersed silica samples (aerosil A-300) in the form of powder or semitransparent plates (~100 μm thick and with a surface area of 10 × 5 mm^2), which were obtained by pressing the initial powder samples [4]. The activation of sample surfaces was carried out by

0023-1584/00/4102-0242$25.00 © 2000 MAIK "Nauka/Interperiodica"

the method proposed by Morterra and Low [5], which enables the formation of so-called reactive silica (RSi). Details of this technique can be found in [4, 6]. The use of filmed samples enabled quantitative spectral measurements in the optical and IR regions to be made. The registration of IR spectra was carried out by placing the samples into a special cell with windows made of IR-transparent silicon plates. ESR measurements were carried out with powdered and filmed samples. All spectra were recorded in vacuum or in a controlled atmosphere.

IR spectra were measured at room temperature using a Digilab Fourier-transform spectrometer. The number of scans was 256–1024, and the resolution was 4 cm^{-1}. ESR spectra were recorded with a 3-cm-range instrument at 77 or 295 K.

The purity of gases used in this work (O_2, C_2H_6, C_2H_4, and CO) was at least 95%. The conditions for the chemisorption of various gases by a sample ensured their absorption to the degree of at least 50% of their initial amount in the gas phase. Therefore, we may assume that the main portion of the products formed in the reaction is irrelevant to the effect of the impurities.

Ab initio calculations were carried out with Gaussian 94 [7]. Molecular models of surface structures were used. Radtsig [8] has reported the experimental data showing that the physicochemical characteristics of $(\equiv Si–O)_2SiXY$ on the silica surface are close to those of its low-molecular analogs, where ≡Si–O groups are replaced by fluorine atoms (F_2SiXY). This enabled us to use fluorine-substituted molecules and radicals in the modeling of the properties of the surface groups of silica. Besides that, for low-molecular systems, quantum-chemical calculations can be carried out at a higher level. Therefore, we used these models.

Geometries of molecules and radicals were optimized by minimizing the gradient norm using the DFT method in the B3LYP/6-311G** approximation [9, 10]. Vibrational spectra of equilibrium structures and transition states were calculated using the harmonic approximation. Transition states had one negative eigenvalue of the Hessian matrix.

To find a correction $\nu(1)_{corr}$ for the calculated $\nu(1)_{calc}$ value of normal vibration, we calculated (at the same theoretical level) the frequency of analogous vibration in a molecule with a similar structure $\nu(2)_{calc}$ for which experimental data were available $\nu(2)_{exp}$. Then, the correction was introduced as follows:

$$\nu(1)_{corr} = \nu(1)_{calc}\{\nu(2)_{exp}/\nu(2)_{calc}\}. \quad (1)$$

This value was compared to the experimental data.

1. SYNTHESIS OF ORGANOSILICON PEROXO RADICALS

The main type of defects stabilized on the surfaces of thermally activated silica samples (RSi) are diamagnetic silylene groups $(\equiv Si–O)_2Si:$ [4, 11]. Their concentration is about $\sim 10^{13}$ cm^{-2}. On the surface of activated samples, paramagnetic radicals $(\equiv Si–O)_3Si^{\cdot}$ are also stabilized in a small amount ($\approx 10^{11}$ cm^{-2}) [4, 11].

Peroxo radicals $(\equiv Si–O)_2Si(C_2H_5)(O–O^{\cdot})$ (**B**) were synthesized in two steps: the formation of silyl radicals $(\equiv Si–O)_2Si^{\cdot}(C_2H_5)$ (**A**) containing a hydrocarbon fragment as one of the substituents and the oxidation of these radicals by molecular oxygen at 200 K.

Radicals **A** are formed by the addition of a low-molecular ethyl radical to the silylene groups [3]:

$$(\equiv Si–O)_2Si: + {}^{\cdot}C_2H_5 \longrightarrow (\equiv Si–O)_2Si^{\cdot}–C_2H_5 \quad (I)$$

Ethyl radicals were obtained from ethane by two methods:

(1) Freshly prepared RSi samples containing $(\equiv Si–O)_3Si^{\cdot}$ radicals were converted into their oxy form using N_2O as an oxidant [12],

$$(\equiv Si–O)_3Si^{\cdot} + N_2O \longrightarrow (\equiv Si–O)_3Si–O^{\cdot} + N_2$$

Oxysilyl radicals are highly reactive toward saturated hydrocarbon molecules, and they abstract hydrogen atoms (even from methane at 77 K) [13]. Their reaction with ethane molecules yields ethyl radicals [3, 13]:

$$(\equiv Si–O)_3Si–O^{\cdot} + C_2H_6 \longrightarrow (\equiv Si–O)_3Si–O–H + {}^{\cdot}C_2H_5$$

Silylene groups are inactive toward ethane (at least at room temperature), but they are efficient acceptors of various radicals [2, 3]. The addition of ethyl radicals to silylene groups is accompanied by the formation of silicon-centered radicals (see reaction (I)).

(2) Ethyl radicals can be generated by diamagnetic dioxasilirane groups [14]. The RSi sample was initially treated in the hydrogen atmosphere ($\approx 10^{-4}$ torr) at 800 K. This treatment removed paramagnetic centers $(\equiv Si–O)_3Si^{\cdot}$ and preserved silylene groups. Dioxasilirane groups were prepared by the oxidation of a small amount (several percents) of silylene centers by molecular oxygen at room temperature [4, 11]:

$$(\equiv Si–O)_2Si: + O_2 \longrightarrow (\equiv Si–O)_2Si\langle{}^{O}_{O} \quad (II)$$

These groups readily react with ethane molecules. According to [14], the reaction occurs as follows:

$$(\equiv Si–O)_2Si\langle{}^{O}_{O} + C_2H_6 \longrightarrow (\equiv Si–O)_2Si\langle{}^{O^{\cdot}}_{OH} + {}^{\cdot}C_2H_5, \quad (III)$$

$$(\equiv Si\text{–}O)_2Si\begin{matrix}O^{\bullet}\\OH\end{matrix} + C_2H_6$$
$$\longrightarrow (\equiv Si\text{–}O)_2Si\begin{matrix}OH\\OH\end{matrix} + {}^{\bullet}C_2H_5 \qquad \text{(III')}$$

Thus, ethyl radicals are generated, and diamagnetic silylene groups accept them (see reaction (I)).

Ethyl radicals also react with dioxasilirane groups to form hydrocarbon radicals [13]:

$$(\equiv Si\text{–}O)_2Si\begin{matrix}O\\O\end{matrix} + {}^{\bullet}C_2H_5$$
$$\longrightarrow (\equiv Si\text{–}O)_2Si\begin{matrix}OH\\O\text{–}CH_2\text{–}H_2C^{\bullet}\end{matrix}$$

The activities of two different diamagnetic groups are comparable and the ratio between the products of reactions (II) and (III) are determined by the concentrations of silylene and dioxasilirane groups on the sample surface. At a coverage of ~5%, more than 95% of radical products is formed via reaction (I). This method enabled an increase in the concentration of radicals in the sample by a factor of 10 as compared to the first method. The second method for generating organosilicon radicals was the main method used in this work.

Figure 1 shows the ESR spectrum of the radicals $(\equiv Si\text{–}O)_2Si^{\bullet}\text{–}CH_2\text{–}CH_3$. In the low- and high-field parts of the spectrum (Fig. 1b), we registered two satellite bands assigned to the paramagnetic centers containing the ^{29}Si isotope ($I = 1/2$) whose natural content is 4.7%. The shape of these bands shows that the hyperfine interaction (HFI) tensor of an unpaired electron with the ^{29}Si nucleus is close to axially symmetric with $a_{iso} = -(29.1 \pm 0.1)$ mT, $b_1 \cong b_2 = (2.1 \pm 0.05)$, and $b_3 = -(4.2 \pm 0.1)$ mT. The values of the HFI constants for unpaired electrons and the silicon nucleus in this radical point to the fact that the spin density is basically localized on the silicon atom. That is, this radical is indeed of the silyl type.

The central part of the ESR spectrum (295 K) is an asymmetric band with the traces of a hyperfine structure (hfs) (Fig. 1a). At 77 K, the form of the central part of the spectrum reversibly changes. The total width of the spectrum increases, and several distinct hfs components appear at a distance of several tenths of a mT due to the protons of ethyl group. Thus, with a decrease in temperature, the unpaired electron–proton HFI constants increase. Reversible changes in the shape of the ESR spectrum with temperature are associated with restricted C_2H_5 rotation.

Figure 2 shows the equilibrium geometry calculated for $F_2Si^{\bullet}\text{–}CH_2\text{–}CH_3$ (**I**), which served as a molecular model of surface centers. Tables 1–4 show geometric and spectral characteristics for this radical. The DFT method gives adequate results when calculating radiospectroscopic characteristics of paramagnetic centers [15]. Table 2 shows that the calculation correctly describes the constants of the HFI of unpaired electron and the ^{29}Si nucleus in this radical. The constants of HFI with protons depend on the spatial configuration of an ethyl fragment in the radical in a complicated manner. Analysis of these dependences and relevant experimental data for the $(\equiv Si\text{–}O)_2Si^{\bullet}\text{–}CH_3$ radical will be reported elsewhere. Here, we only note that the calculation, which agrees with the experiment, suggests that freezing out the internal rotations around the Si–C bond in the radical results in a substantial decrease in the HFI constant of the electron with the protons of the methylene group.

The formation of radicals **A** is accompanied by the appearance of IR bands in the region of C–H stretching vibrations (Fig. 3a, spectrum *1*). If radicals were prepared according to the second method, the IR spectrum contained a band at 3746 cm^{-1} (not shown in Fig. 3), which is relevant to the formation of an O–H group [16] in the course of reaction (III'). Several bands in the region of C–H stretching vibrations belong to the bonds of the hydrocarbon fragment in the $(\equiv Si\text{–}O)_2Si^{\bullet}\text{–}CH_2\text{–}CH_3$ radical. There are two intense bands at 2973 and 2890 cm^{-1}.

Table 4 describes the vibrational spectrum of radical **I**. For empirical correction (1) of the calculated frequencies, we used the D_3CCHD_2 molecule with $\nu_{exp}(C\text{–}H) = 2950$ cm^{-1} [17] and $\nu_{calc}(C\text{–}H) = 3066$ cm^{-1}. Upon correction, the frequencies of C–H stretching vibration for the methylene group **I** were 2916 and 2900 cm^{-1} and, for the methyl group, 2985, 2973, and 2916 cm^{-1}. According to the calculation and experimental data, the intensity of stretching for the Si–H and C–H bonds in organosilicon compounds changes in the following manner: Si–H $\gg$ Si–C–H $<$ Si–C–C–H. Two bands with comparable intensities near 2960 and 2890 cm^{-1} are characteristic of antisymmetric and symmetric stretching vibrations of the C–H bond in the methyl group of hydrocarbons [18]. Thus, two intense bands at 2973 and 2890 cm^{-1} should be assigned to analogous vibrations in the methyl group of the radical **A**. Other, less intensive bands are likely due to the stretching vibrations of the methylene group in the radical.

The peroxo radicals **B** were obtained by the oxidation of radicals **A** by molecular oxygen at $\approx 10^{-3}$ torr and 200 K:

$$(\equiv Si\text{–}O)_2Si^{\bullet}\text{–}CH_2\text{–}CH_3 + O_2$$
$$\longrightarrow (\equiv Si\text{–}O)_2Si\begin{matrix}O\text{–}O^{\bullet}\\CH_2\text{–}CH_3\end{matrix} \qquad \text{(IV)}$$

Under these conditions, oxygen only reacts with radical centers, and the process is accompanied by the almost complete transformation of silyl radicals into

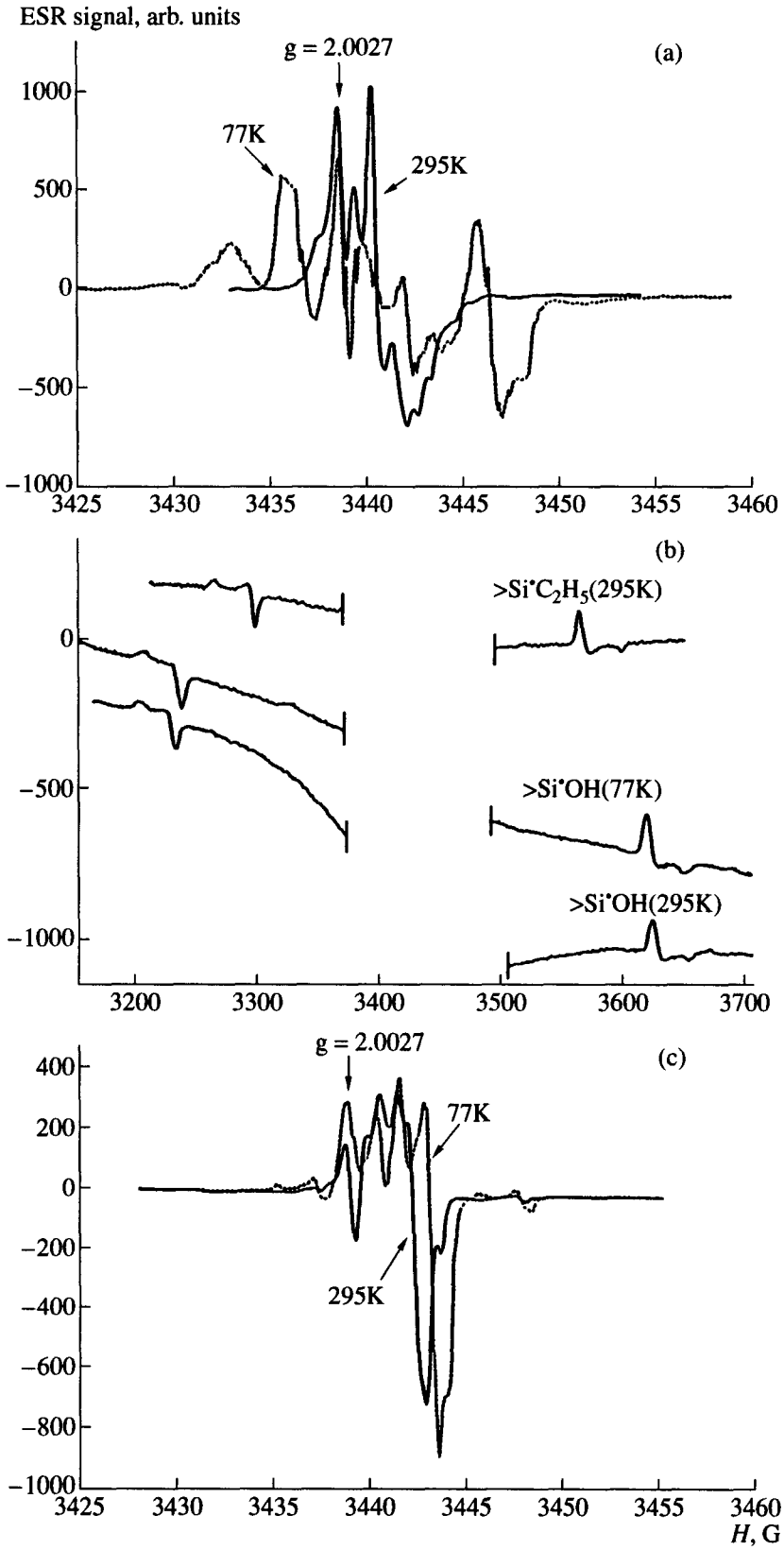

Fig. 1. ESR spectra of radicals at 77 (dashed lines) and 295 K (solid lines). The singlet signal with $g = 2.0027$ is due to an impurity signal: (a) $(\equiv Si–O)_2{}^{28}Si^{\bullet}(C_2H_5)$, (b) $(\equiv Si–O)_2{}^{29}Si^{\bullet}(C_2H_5)$ and $(\equiv Si–O)_2{}^{29}Si^{\bullet}–O–H$, and (c) $(\equiv Si–O)_2{}^{28}Si^{\bullet}–O–H$.

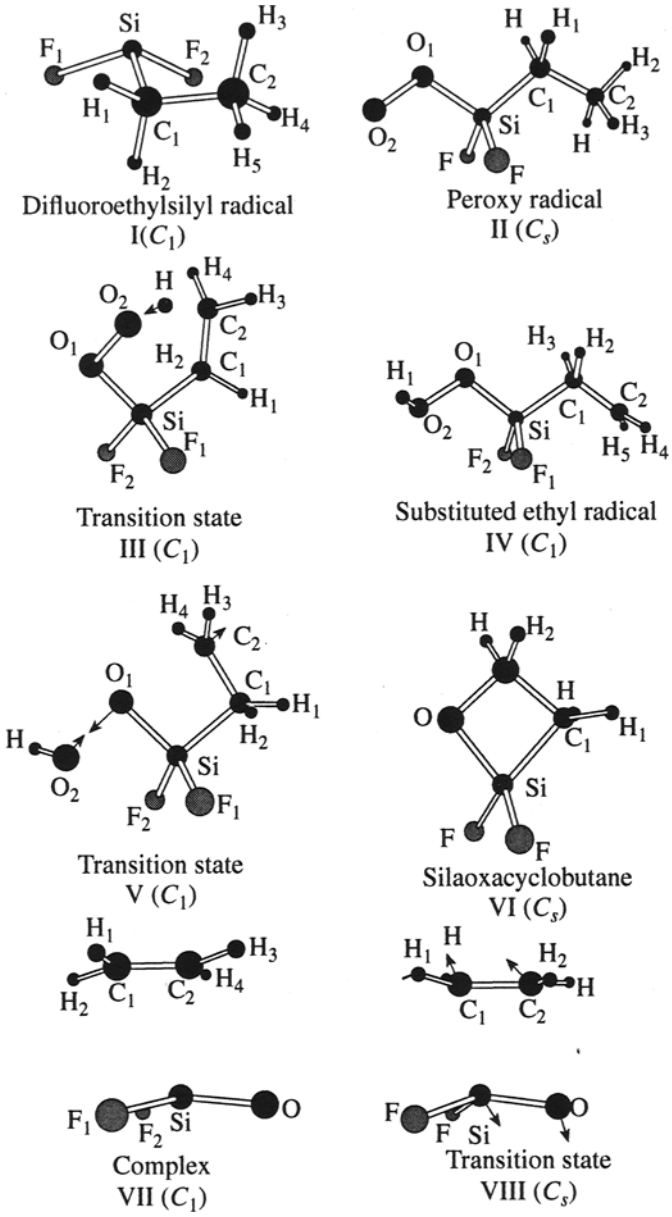

Fig. 2. Spatial configurations, symmetry, and atom numbering in molecules and radicals.

their peroxo form. As this takes place, a characteristic signal appears in the ESR spectrum from the organosilicon peroxo radicals [19]. The shape of this signal is stipulated by the anisotropy of the g-tensor (at 77 K, $g_1 = 2.002$, $g_2 = 2.010$, and $g_3 = 2.068$). In the spectra registered at room temperature, this is a broad singlet band with a g-factor of ~2.026. Reversible changes in the ESR spectrum shape with temperature are stipulated by freezing out the rotation of the oxygen fragment along the Si–O bond.

The formation of the peroxo radical changes the IR spectrum in the region of C–H bond stretching (Fig. 3a, spectrum *2*). These changes are band shifts (by ~6 cm^{-1}) in the higher wavenumber region. Because the oxidation reaction involves only the radical centers, these experimental data support the conclusion that the bands at 2800–3000 cm^{-1} belong to radicals **A** and **B**.

Figure 2 shows the equilibrium structure of $F_2Si(C_2H_5)(O–O^{\bullet})$ radical (**II**), which is a molecular model of the corresponding surface center. The calculation shows that the formation of a peroxo radical results in a small (several reciprocal centimeters) shortwave shift of the C–H vibration frequencies in the ethyl fragment (see Table 4).

2. THERMAL TRANSFORMATIONS OF PEROXO RADICALS

The transformation of peroxo radicals starts when the sample is heated to room temperature. Figure 4 shows a kinetic curve in the coordinates of the first-order rate law. The concentration of peroxo radicals decreases. The rate constant determined from the slope of the straight line is $k_{app}(296\ K) = (1 \pm 0.1) \times 10^{-3}\ s^{-1}$.

A decrease in the concentration of peroxo radicals is accompanied by the appearance of a new paramagnetic center. This ESR spectrum is shown in Figs. 1b and 1c. The transformation of radical centers occurs with the conservation of their overall concentration (within the limits of measurement accuracy, which is not worse than 20%). The ESR signal observed belongs to the free radical $(\equiv Si–O)_2Si^{\bullet}–OH$ (**C**) [20]. This is evident from its spectroscopic characteristics. (1) In the low- and high-field parts of the spectrum, two satellite bands are present (Fig. 1b), which are characteristic of paramagnetic centers containing the α-^{29}Si atom (I = 1/2; the natural concentrations is 4.7%). The HFI tensor of an unpaired electron with the ^{29}Si nucleus is axially symmetric. At 295 K, the principal components of the HFI tensor are $a_{iso} = -(41.4 \pm 0.1)$ mT, $b_1 = b_2 = (1.85 \pm 0.05)$, and $b_3 = -(3.7 \pm 0.05)$ mT. At 77 K, the isotropic constant decreases: $a_{iso} = -(40.6 \pm 0.1)$ mT, $b_1 = b_2 = (1.85 \pm 0.05)$, and $b_3 = -(3.7 \pm 0.05)$ mT. (2) The form of the central portion of the spectrum reversibly changes when changing the registration temperature from 300 to 77 K (Fig. 1c). These changes are stipulated by freezing out the O–H group rotation in the radical with a temperature increase. All these properties are characteristic of radicals **C** [20]. We reported earlier the results of quantum chemical calculations of the radiospectroscopic characteristics of the radicals of this type [21]. These results agree well with the experimental data.

Figures 3b and 3c show the differential IR spectra of a sample containing radicals **B** and a sample that was kept for a long time at room temperature. This treatment of the second sample results in a complete decay of radicals **B**. We observed two new bands in the IR spectrum in two spectral ranges. A band at 3715 cm^{-1} (Fig. 3b) is in the spectral range, which is characteristic of stretching vibrations of the O–H bonds in hydroxyl groups bound to the silicon atom. The intensity of this

Table 1. Optimized geometries*

No.	Structure	Parameters
1	$F_2Si{=}O$ (C_{2v})	$R(SiO) = 1.510$, $R(SiF) = 1.586$, $\angle OSiF = 127.9$
2	$H_2C{=}CH_2$ (D_{2h})	$R(CC) = 1.327$, $R(CH) = 1.085$, $\angle HCC = 121.8$
3	$F_2Si^{\cdot}C_2H_5$ (C_1, **I**)	$R(SiC_1) = 1.891$, $R(SiF_1) = 1.6244$, $R(SiF_2) = 1.625$, $R(CC) = 1.536$, $R(C_1H_1) = 1.094$, $R(C_1H_2) = 1.098$, $R(C_2H_3) = 1.093$, $R(C_2H_4) = 1.092$, $R(C_2H_5) = 1.093$, $\angle C_1SiF_1 = 107.7$, $\angle FSiF = 105.8$, $\angle SiC_1C_2 = 114.3$, $\angle SiC_1H_1 = 108.0$, $\angle SiC_1H_2 = 104.8$, $\angle C_1C_2H_3 = 111.6$, $\angle C_1C_2H_4 = 111.3$, $\angle C_1C_2H_5 = 110.8$, $\angle FSiC_1C_2 = 170.1$, $\angle SiC_1C_2H_1 = 61.6$, $\angle H_1C_1C_2H_3 = -60.2$, $\angle F_1SiC_1F_2 = 113.6$, $\angle H_2C_1C_2H_1 = -118.9$, $\angle H_4C_2C_1H_3 = -120.4$, $\angle H_5C_2C_1H_3 = -119.8$
4	$F_2Si(OO^{\cdot})(C_2H_5)$ (C_s, **II**)	$R(SiO_1) = 1.709$, $R(OO) = 1.349$, $R(SiF) = 1.600$, $R(SiC_1) = 1.842$, $R(CC) = 1.543$, $R(C_1H_1) = 1.095$, $R(C_2H_2) = 1.092$, $R(C_2H_3) = 1.092$, $\angle OOSi = 111.9$, $\angle OSiC = 107.7$, $\angle SiCC = 113.9$, $\angle SiC_1H_1 = 107.7$, $\angle C_1C_2H_2 = 110.5$, $\angle C_1C_2H_3 = 111.4$, $\angle OOSiF = 57.7$, $\angle OSiC_1H_1 = 57.0$, $\angle SiC_1C_2H_3 = 60.2$
5	$F_2SiO_2C_2H_5$ (C_1, **III**)	$R(SiO_1) = 1.671$, $R(OO) = 1.439$, $R(SiF_1) = 1.601$, $R(SiF_2) = 1.600$, $R(SiC_1) = 1.877$, $R(CC) = 1.513$, $R(C_1H) = 1.364$, $R(O_2H) = 1.190$, $R(C_1H_1) = 1.094$, $R(C_1H_2) = 1.094$, $R(C_2H_3) = 1.087$, $R(C_2H_4) = 1.088$, $\angle OOSi = 104.4$, $\angle OSiC = 106.9$, $\angle SiCC = 110.9$, $\angle OOH = 103.3$, $\angle OHC_2 = 156.2$, $\angle HC_2C_1 = 104.3$, $\angle C_2C_1H_1 = 111.7$, $\angle C_2C_1H_2 = 111.5$, $\angle C_1C_2H_3 = 116.3$, $\angle C_1C_2H_4 = 116.5$, $\angle CSiF_1 = 111.7$, $\angle CSiF_2 = 112.8$, $\angle CSiOO = -56.4$, $\angle SiOOH = 58.9$, $\angle OOHC = -50.6$, $\angle OHCC = 16.0$, $\angle HCCSi = -1.5$, $\angle CCSiO = 26.6$, $\angle CSiF_1O = 120.2$, $\angle CSiF_2O = -116.7$, $\angle H_1C_1C_2H_3 = -12.1$, $\angle H_2C_1C_2H_3 = -132.7$, $\angle H_3C_2C_1Si = 108.8$, $\angle H_4C_2C_1Si = -112.5$
6	$F_2Si(OOH)(CH_2{-}CH_2^{\cdot})$ (C_1, **IV**)	$R(SiO) = 1.668$, $R(OO) = 1.468$, $R(OH_1) = 0.968$, $R(SiF_1) = 1.607$, $R(SiF_2) = 1.603$, $R(SiC) = 1.865$, $R(CC) = 1.488$, $R(C_1H_2) = 1.095$, $R(C_1H_3) = 1.096$, $R(C_2H_4) = 1.082$, $R(C_2H_5) = 1.082$, $\angle H_1OO = 99.6$, $\angle OOSi = 108.7$, $\angle OSiC = 107.5$, $\angle SiCC = 111.0$, $\angle CSiF_1 = 111.8$, $\angle CSiF_2 = 111.4$, $\angle H_2C_1Si = 111.0$, $\angle H_3C_1Si = 106.9$, $\angle H_4C_2C_1 = 120.5$, $\angle H_5C_2C_1 = 120.5$, $\angle H_1OOSi = 120.1$, $\angle OOSiC = 177.5$, $\angle OSiCC = 179.4$, $\angle OSiF_1C = -119.1$, $\angle OSiF_2C = 119.6$, $\angle OC_1SiH_2 = 56.8$, $\angle OC_1SiH_3 = -58.4$, $\angle H_4C_2C_1Si = -86.0$, $\angle H_5C_2C_1Si = 84.1$
7	$F_2SiO_2C_2H_5$ (C_1, **V**)	$R(SiO) = 1.652$, $R(OO) = 1.696$, $R(OH) = 0.968$, $R(SiF_1) = 1.602$, $R(SiF_2) = 1.607$, $R(SiC) = 1.882$, $R(CC) = 1.482$, $R(O_1C_2) = 2.258$, $R(C_1H_1) = 1.092$, $R(C_1H_2) = 1.092$, $R(C_2H_3) = 1.081$, $R(C_2H_4) = 1.081$, $\angle HOO = 95.5$, $\angle OOSi = 91.1$, $\angle OOC_2 = 169.5$, $\angle OC_2C_1 = 88.0$, $\angle OSiC = 97.3$, $\angle SiCC = 96.2$, $\angle CSiF_1 = 111.7$, $\angle CSiF_2 = 111.2$, $\angle H_1C_1Si = 111.4$, $\angle H_2C_1Si = 111.6$, $\angle H_3C_2C_1 = 121.0$, $\angle H_4C_2C_1 = 120.9$, $\angle HOOSi = -117.3$, $\angle OOSiC = -177.7$, $\angle OSiCC = -2.1$, $\angle CSiF_1O = 110.0$, $\angle CSiF_2O = -108.5$, $\angle H_1C_1SiO = 116.1$, $\angle H_2C_1SiO = -120.4$, $\angle H_3C_2C_1Si = 95.0$, $\angle H_4C_2C_1Si = -94.7$
8	$F_2SiOC_2H_4$ (C_s, **VI**)	$R(SiO) = 1.652$, $R(SiF) = 1.603$, $R(SiC_1) = 1.855$, $R(SiC_2) = 2.259$, $R(OC_2) = 1.477$, $R(C_2C_1) = 1.558$, $R(C_1H_1) = 1.089$, $R(C_2H_2) = 1.090$, $\angle CSiF = 119.3$, $\angle OSiC_1 = 83.9$, $\angle SiC_1C_2 = 82.4$, $\angle C_1C_2O = 101.4$, $\angle C_2OSi = 92.3$, $\angle H_1C_1Si = 116.9$, $\angle H_2C_2C_1 = 113.6$, $\angle OSiFC_1 = 97.0$, $\angle OSiC_1H_1 = 113.4$, $\angle H_2C_2C_1Si = 116.5$
9	$F_2SiOC_2H_4$ (C_1, **VII**)	$R(SiO) = 1.519$, $R(SiF_1) = 1.605$, $R(SiF_2) = 1.603$, $R(SiC_1) = 2.586$, $R(SiC_2) = 2.403$, $R(OC_2) = 2.897$, $R(CC) = 1.346$, $R(C_1H_1) = 1.084$, $R(C_1H_2) = 1.084$, $R(C_2H_3) = 1.083$, $R(C_2H_4) = 1.085$, $\angle OSiF_1 = 125.0$, $\angle OSiF_2 = 125.5$, $\angle OSiC_1 = 120.1$, $\angle OSiC_2 = 92.4$, $\angle C_1SiC_2 = 31.0$, $\angle H_1C_1C_2 = 121.5$, $\angle H_2C_1C_2 = 121.6$, $\angle H_3C_2C_1 = 121.9$, $\angle H_4C_2C_1 = 121.3$, $\angle OSiF_1C_1 = 119.9$, $\angle OSiF_2C_1 = -126.7$, $\angle OSiC_1C_2 = 29.7$, $\angle OSiC_1H_1 = -88.4$, $\angle OSiC_1H_2 = 150.7$, $\angle SiC_1C_2H_3 = -97.3$, $\angle SiC_1C_2H_4 = 89.3$
10	$F_2SiOC_2H_4$ (C_s, **VIII**)	$R(SiO) = 1.541$, $R(SiF) = 1.606$, $R(SiC_1) = 2.146$, $R(SiC_2) = 2.334$, $R(OC_2) = 2.358$, $R(CC) = 1.378$, $R(C_1H_1) = 1.084$, $R(C_2H_2) = 1.082$, $\angle OSiF = 122.2$, $\angle OSiC_1 = 107.2$, $\angle SiC_1C_2 = 79.7$, $\angle H_1C_1C_2 = 119.9$, $\angle H_2C_2C_1 = 121.9$, $\angle OSiFC_1 = 115.7$, $\angle H_1C_1SiO = 118.6$, $\angle H_2C_2C_1Si = 93.0$

* The column "structure" indicates the stoichiometric composition of compounds. Their spatial configurations and atom numbering are shown in Fig. 2. Roman numbering corresponds to the numbering of structures in Fig. 2. Bond lengths are in angstroms, and the angels are in degrees. All calculations were carried out using the density functional theory at the B3LYP/6-311G** level. The subscripts in the third column correspond to the numbers of atoms in the structures shown in Fig. 2.

Table 2. Radiospectroscopic characteristics of the $F_2Si^{\cdot}CH_2CH_3$* radical

Atom	a_{iso}	b_1	b_2	b_3
^{29}Si	–28.9	2.52	2.43	–4.96
$^1H_1$	–0.35	–0.29	–0.09	0.38
$^1H_2$	0.99	–0.28	–0.02	0.29
$^1H_3$	0.25	–0.06	–0.03	0.09
$^1H_4$	0.02	–0.10	–0.06	0.16
$^1H_5$	0.03	–0.08	–0.05	0.13

* Numbering of hydrogen atoms in the radical (subscripts) is shown in Fig. 2 (structure **I**). The values (mT) of isotropic (a_{iso}) and anisotropic (three principal values b_1, b_2, and b_3) of the HFI constants are calculated using density functional theory at the UB3LYP/6-311G** level [25].

band increases in proportion to the concentration of radicals **C** (registration with ESR). An analogous band was registered when the other method was used for radical **C** generation—by the addition of hydrogen atoms to the silanone groups [20]:

$$(\equiv Si–O)_2Si=O + H^{\cdot} \longrightarrow (\equiv Si–O)_2Si^{\cdot}–O–H$$

Quantum chemical calculations [21] also point to the low-frequency shift of the O–H bond stretching band in the radical as compared to the terminal surface group of silica (3749 cm^{-1} [5]). Based on these data, we assigned this band to O–H stretching in the $>Si^{\cdot}–OH$ radical.

In one of the runs we prepared a sample which contained diamagnetic groups in the dioxasilirane form (silylene groups in this sample were oxidized by molecular oxygen, see reaction (II)) and peroxo radicals. In this sample, the decay of peroxo radicals occurred at the same rate, but the ESR method registered other paramagnetic products of transformation: the $(\equiv Si–O)_2Si(O^{\cdot})(O–H)$ and $(\equiv Si–O)_2Si(O–O^{\cdot})(O–H)$ radicals.

These experimental data suggest that new paramagnetic centers formed during the reaction are produced by accepting low-molecular radicals, formed by the decomposition of peroxo radicals, by diamagnetic surface groups. The formation of the $(\equiv Si–O)_2Si^{\cdot}–O–H$ radicals in the presence of silylene groups suggests that

Table 3. Electronic and zero-point energies (ZPE)*

No.	Structure	Electronic energy, at.u.	*ZPE*, kcal/mol
1	$F_2Si + {}^{\cdot}C_2H_5$	(–489.34462) + (–79.18365) = –568.18365	2.9 + 37.0 = 39.9
2	$F_2Si^{\cdot}C_2H_5$ (C_1, **I**)	–568.58840	44.4
3	$F_2Si^{\cdot}C_2H_5 + O_2$	(–568.58840) + (–150.36479) = –718.95319	44.4 + 2.3 = 46.7
4	$F_2Si(OO^{\cdot})(C_2H_5)$ (C_s, **II**)	–719.03788	48.8
5	$F_2SiO_2C_2H_5$ (C_1, **III**)	–718.99950	45.2
6	$F_2Si(OOH)(CH_2–C^{\cdot}H_2)$ (C_1, **IV**)	–719.01840	47.1
7	$F_2SiO_2C_2H_5$ (C_1, **V**)	–719.001445	46.7
8	$F_2SiOC_2H_4$ (C_s, **VI**) + ${}^{\cdot}OH$	(–643.29596) + (–75.75453) = –719.05049	41.5 + 5.3 = 46.8
9	$F_2Si=O + H_2C=CH_2$	(–564.61018) + (–78.61398) = –643.22416	5.9 + 31.9 = 37.8
10	$F_2SiOC_2H_4$ (C_1, **VII**)	–643.24567	39.5
11	$F_2SiOC_2H_4$ (C_s, **VIII**)	–643.24073	39.6
12	$F_2SiOC_2H_4$ (C_s, **VI**)	–643.29596	41.5
13	$CH_3CH_2C^{\cdot}H_2 + O_2$	(–118.50782) + (–150.36479) = –268.87261	55.1 + 2.35 = 57.45
14	$CH_3CH_2CH_2OO^{\cdot}$	–268.92629	62.6
15**	TS-1	–268.88175	58.9
16	${}^{\cdot}CH_2CH_2CH_2OOH$	–268.89136	60.45
17***	TS-2	–268.86303	59.95
18	cyclo-C_3H_6O (C_{2v}) + ${}^{\cdot}OH$	(–193.15922) + (–75.75453) = –268.91375	54.5 + 5.3 = 59.8

* The second column shows the stoichiometric composition of compounds. Their spatial configurations and atom numbering are shown in Fig. 2. Roman numbering (in brackets) corresponds to the numbering of structures in Fig. 2. Electronic energies are in atomic units (1 at.u. = 627.5 kcal/mol). Zero-point energies are in kcal/mol. All calculations were carried out using density functional theory at the B3LYP/6-311G** level.

** Transition state for H abstraction from a methyl group by a peroxy radical.

*** Transition state for the reaction of hydroxy radical formation.

Table 4. Vibrational spectra of the structures*

No.	Structure	Positions and intensities of IR bands
1	$F_2Si^{\cdot}C_2H_5$ (C_1, I)	61(0.8), 140(0.6), 196(3.2), 265(15), 308(6.5), 340(12), 621(16), 707(28), 833(143), 883(142), 969(6.1), 979(5.9), 1031(10), 1247(4.9), 1257(0.3), 1420(2.1), 1449(3.9), 1504(6.9), 1508(6.6), 3014(9.0), 3031(28.7), 3068(3.0), 3090(22), 3102(25)
2	$F_2Si(OO^{\cdot})(C_2H_5)$ (C_s, II)	41(0.3), 85(0.0), 109(0.5), 173(0.2), 182(4.7), 244(1.7), 282(4.3), 306(12), 328(25), 425(63), 654(2.5), 711(7.3), 775(192), 907(147), 940(121), 986(11), 1010(65), 1034(41), 1137(72), 1265(3.3), 1298(14), 1425(0.9), 1454(8), 1509(9), 1510(8), 3032(2.3), 3038(29), 3068(1.2), 3104(19), 3106(22)
3	$F_2SiO_2C_2H_5$ (C_1, III)	1670i(331), 40(0.2), 134(1.8), 193(0.3), 257(4.6), 290(13), 303(4.1), 333(26), 407(41), 473(2.6), 600(4.2), 653(6.4), 734(5.9), 814(101), 917(155), 940(134), 968(62), 994(65), 1020(13), 1061(31), 1180(53), 1202(33), 1243(1.2), 1437(0.0), 1466(3), 1526(16), 3037(3.4), 3086(1.3), 3095(8.8), 3185(4.6)
4	$F_2Si(OOH)(CH_2{-}CH_2^{\cdot})$ (C_1, IV)	50(0.3), 94(4.3), 109(1.2), 166(2.5), 173(10), 229(14), 255(57), 276(12), 329(22), 339(55), 416(65), 512(101), 663(0), 715(4.5), 793(122), 890(114), 918(76), 968(83), 983(113), 1064(3), 1185(44), 1249(0.6), 1379(57), 1442(8), 1468(0.4), 3019(4.9), 3069(3.6), 3151(8), 3258(5.8), 3774(68)
5	$F_2SiO_2C_2H_5$ (C_1, V)	628i(530), 78(0.3), 115(5.5), 159(4.4), 212(1.3), 229(5.4), 286(11), 302(25), 345(87), 399(82), 431(40), 476(0.3), 655(29), 735(2.9), 785(4.1), 818(19), 894(28), 956(179), 970(163), 1062(35), 1074(71), 1115(60), 1238(0.4), 1449(1.4), 1486(3.4), 3054(3.6), 3116(1.8), 3165(5.8), 3272(1.1), 3789(98)
6	$F_2SiOC_2H_4$ (C_s, VI)	126(0), 186(0.2), 294(16), 301(15), 328(26), 538(23), 719(2.1), 752(37), 825(92), 882(16), 925(101), 935(53), 965(173), 992(167), 1133(88), 1170(0), 1217(0.6), 1338(6.4), 1453(15), 1523(0), 3066(41), 3090(3.7), 3119(16), 3149(8.8)
7	$F_2SiOC_2H_4$ (C_1, VII)	63(0.2), 133(5.3), 159(1.4), 186(15), 213(2.1), 318(33), 330(10), 367(229), 418(1.7), 779(52), 837(1), 924(156), 1001(6.7), 1040(82), 1063(7.4), 1241(0.2), 1285(116), 1370(1.6), 1479(17), 1643(1.8), 3142(0.3), 3148(0.5), 3226(0.4), 3250(0.3)
8	$F_2SiOC_2H_4$ (C_s, VIII)	249i(20), 57(1.2), 259(4.1), 336(31), 337(8.4), 376(16), 418(195), 568(0), 785(76), 831(1.3), 908(?), 925(162), 993(5.6), 1057(5.6), 1200(115), 1242(0), 1312(76), 1479(15), 1578(18), 3133(5), 3175(0.7), 3224(0.2), 3270(1.8)

* The second column shows the stoichiometric composition of compounds. Their spatial configurations are shown in Fig. 2. Roman numbering (in brackets) corresponds to the numbering of structures in Fig. 2. Frequencies are in reciprocal centimeters, and the intensities of IR bands are in km/mol (in brackets). Calculations were carried out using density functional theory at the B3LYP/6-311G** level. The calculated frequencies are not scaled.

low-molecular radicals are hydroxyls:

$$(\equiv Si{-}O)_2Si{:} + {}^{\cdot}OH \longrightarrow (\equiv Si{-}O)_2Si^{\cdot}{-}OH \quad (V)$$

The reaction is accompanied by the restructuring of the IR spectrum in the region of C–H stretching (Fig. 3c). The bands at 2979 and 2896 cm^{-1} disappear, and new bands appear at 3017, 2989, and 2919 cm^{-1}. The latter are due to the stretching vibrations of the C–H bonds in silaoxacyclobutane $>Si\langle{}^{O}_{CH_2}\rangle CH_2$ (**D**). These groups can be synthesized on the silica surface by other chemical reactions. We found that they have identical IR spectra in this spectral region.

3. PRODUCTS OF REACTION $(\equiv Si{-}O)_2Si{=}O + H_2C{=}CH_2$

Radtsig and co-workers [22, 23] have shown that the silanone groups $(\equiv Si{-}O)_2Si{=}O$ stabilized on the silica surface react with acetylene molecules. The reaction is accompanied by the addition of an acetylene molecule to the π-bond of a silanone group to form a four-membered cyclic structure $>Si\langle{}^{O}_{CH}\rangle CH$. Ethylene molecules are also active in the reactions with silanone groups. The rate constant of this reaction is $k(298\ K) \geq 3 \times 10^{-17}$ cm^3 $molecule^{-1}$ s^{-1}. This allows us to estimate the apparent activation energy of the process: $E_{app} = (2 \pm 2)$ kcal/mol (for more details, see [23]).

Figure 3d shows the differential IR spectrum of the silica sample, which initially contained the >Si=O groups (they have a band at 1306 cm^{-1} [22]) and was then treated with ethylene. As a result of ethylene chemisorption, silanone groups disappear, and new bands appear in the region of C–H stretching vibrations at 3017, 2989, 2972(?), and 2919 cm^{-1}. The positions and ratios of their intensities are analogous to those of

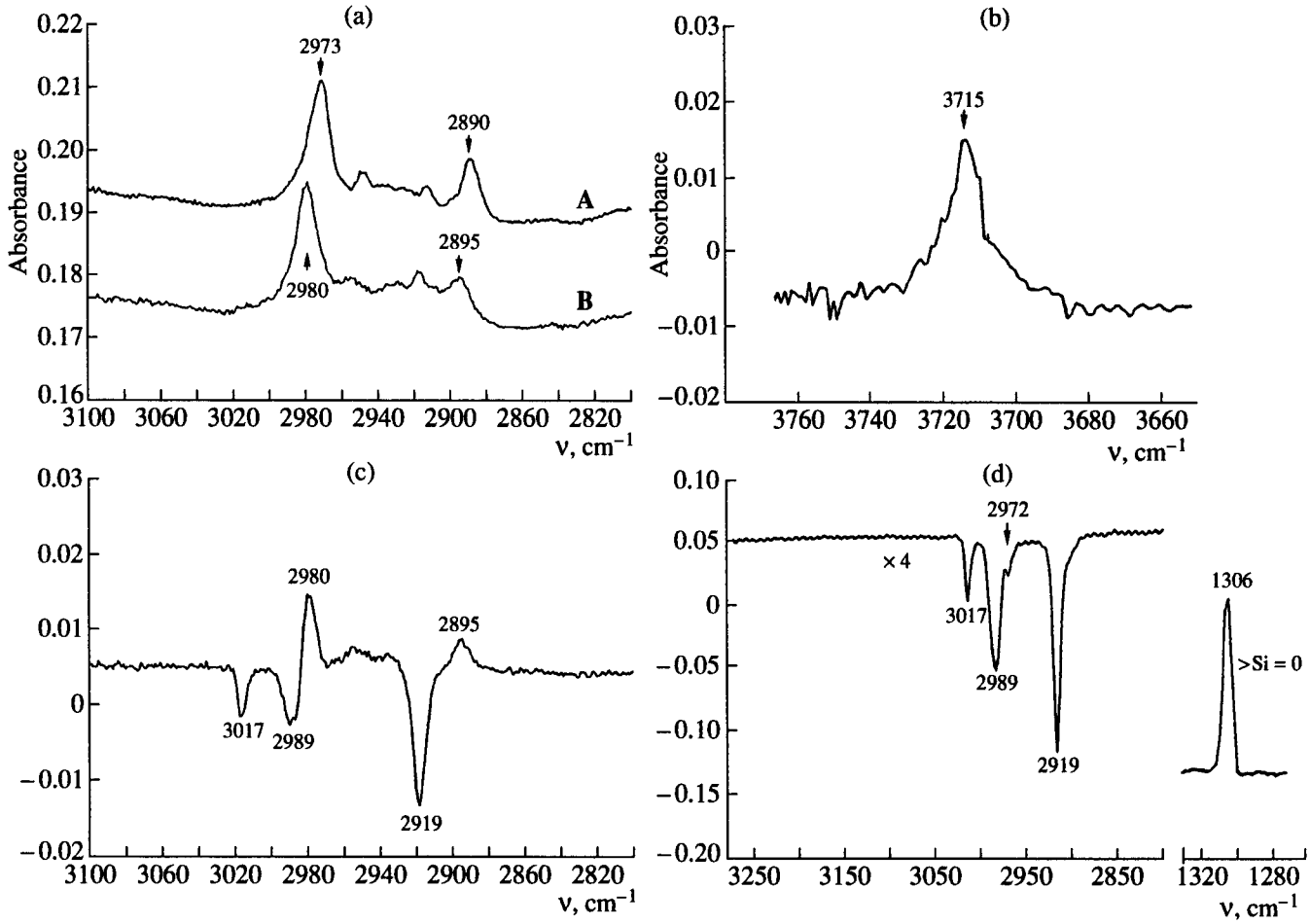

Fig. 3. IR spectra of surface groups (295 K): (a) radicals $(\equiv Si–O)_2Si^{\cdot}(C_2H_5)$ (**A**) and $(\equiv Si–O)_2Si(C_2H_5)(O–O^{\cdot})$ (**B**); (b) radicals $(\equiv Si–O)_2Si^{\cdot}O–H$ (**C**) in the stretching vibration region of the O–H group; (c) differential spectrum obtained by subtracting from the spectrum of the sample with $(\equiv Si–O)_2Si(C_2H_5)(O–O^{\cdot})$ radicals the spectrum of the same sample after thermal decomposition of these radicals; (d) differential spectrum obtained by subtracting from the spectrum of the sample with $(\equiv Si–O)_2Si–O$ groups the spectrum of the same sample after treatment with ethylene molecules. The band of the >Si=O group (1306 cm^{-1}) is shown separately.

the bands formed by the thermal transformation of peroxo radicals **B**.

Proceeding from the chemical properties of reacting molecules, we may expect that the reaction is accompanied by the addition of a silanone group to the double bond of an ethylene molecule:

$$(\equiv Si–O)_2Si=O + CH_2=CH_2 \longrightarrow (\equiv Si–O)_2Si\begin{matrix}O\\ \diagdown\diagup\\ CH_2\end{matrix}\!\!\begin{matrix}\diagup\\ \diagdown\\ CH_2\end{matrix} \quad \text{(VI)}$$

Quantum chemical calculations support this hypothesis. Figure 2 shows the structure of the $F_2Si < OC_2H_4$ molecule (**VI**) and Tables 1, 3, and 4 specify its characteristics. For the empirical correction (1) of calculated C–H stretching frequencies in the $F_2SiOC_2H_4$ molecule, we used the frequencies of C–H stretching frequencies in the cyclo-$(CH_2)_3O$ molecule [24]. For the methylene group bound to two carbon atoms ν_{exp}(C–H) = 3006.5 and 2935 cm^{-1}, ν_{calc}(C–H) = 3124 and 3070 cm^{-1}. For the methylene group bound to oxygen, ν_{exp}(C–H) = 2935 and 2890 cm^{-1} and ν_{calc}(C–H) = 3049 and 3007 cm^{-1}. After appropriate corrections, the frequencies of $C(1)H_2$ bond stretching vibrations in a $F_2SiOC_2H_4$ molecule became 3030 and 2977 cm^{-1}. For the $C(2)H_2$ bond, the corrected values are 3003 and 2947 cm^{-1}. On the average, the calculated values are overestimated by 15 cm^{-1} as compared to the experimental values. This is probably due to the somewhat inappropriate choice of the reference molecule. The $C(1)H_2$ bonds are characterized by higher values of vibration frequencies and lower intensities. The fact that the vibration frequencies of $C(2)H_2$ bonds are lower may be due to the effect of an electronegative substituent (oxygen).

Using the methods of quantum chemistry, the mechanism of reaction (VI) was analyzed. Figure 5 shows the energy diagram of this process. The silanone group reacts with CO_2, N_2O, and HC≡CH molecules in a similar way [23]. First, a relatively stable (–11.8 kcal/mol) intermolecular complex (**VII**) is formed. Figure 2 shows its structure, which is typical of the π-complex

formed by a low-coordinated silicon atom of the silanone group and the π-bond of the ethylene molecule. Some portion of the electron density (0.14e) of the ethylene molecule transfers to the silanone molecule (a donor and acceptor, respectively). The low-coordinated silicon atom mediates this transfer. However, in the silanone molecule, this charge is distributed between the electronegative substituents of the silicon atom (oxygen and fluorine), whereas the charge of the silicon atom remains virtually unchanged.

Figure 2 shows the "complex–cycle" transition state (**VIII**). The arrows point to the directions of atomic shifts as the system moves along the reaction coordinate. The transition state is well below the states of isolated molecules, and the corresponding activation barrier is small. Thus, the rate-limiting step of the process is the step of intermolecular complex formation. The experimental activation energy of this reaction is 2 ± 2 kcal/mol.

To complete this section, we note that the cyclic compound **D** was synthesis by another method, namely by the reaction of ethylene oxide with the surface silylene centers:

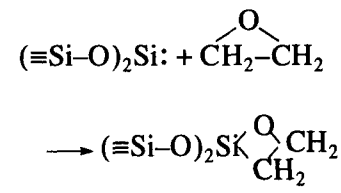

This reaction occurs at room temperature (it was controlled by a decrease in the concentration of silylene centers in a sample). IR spectroscopy registered analogous adsorption bands in the region of C–H stretching vibrations for the products of this reaction.

4. MECHANISM OF HYDROXY RADICAL FORMATION

The products of the transformation of peroxy radical **B** contain hydroxy radicals and silaoxacyclobutane **D**. This suggests the following mechanism of their formation:

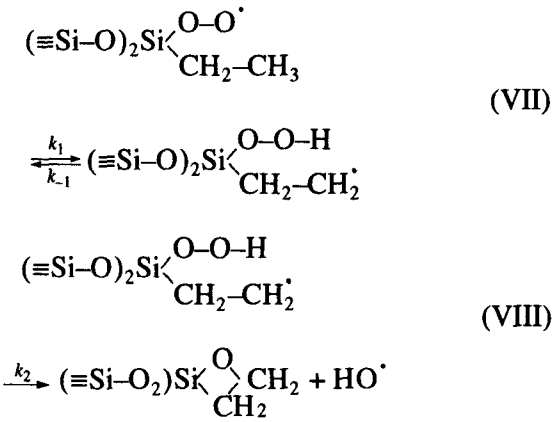

(VII)

(VIII)

According to this scheme, the intramolecular transfer of the hydrogen atom forms a hydroperoxy group and an alkyl radical. Then, the O–O bond of the hydroperoxy group cleaves, being attacked by a radical. This is accompanied by the formation of a hydroxy radical and by the formation of a diamagnetic four-membered ring. The diamagnetic groups on the solid surface are accepted by the hydroxy radicals resulting in the stabilization of the corresponding radical product. Both steps (intramolecular H atom transfer and the elimination of the hydroxy radical) occur via cyclic transition states.

The data on the energetic barriers of the separate steps of such a process were obtained by quantum chemical calculations. The properties of silicon-containing systems are often compared to their carbon-containing analogs. On the one hand, this allows better understanding of specific features in the system behavior, which are stipulated by the presence of silicon atoms. On the other hand, this makes it possible to correct the calculated results, because carbon-containing systems are studied better. Therefore, in parallel with the calculation of silicon-containing systems, we calculated the characteristics of analogous processes with hydrocarbon (the F_2Si group was replaced by the CH_2 group). Data are available on the values of the activation barriers for these processes with hydrocarbons [25]. This is also useful for the critical analysis of the results of quantum chemical calculations. Figure 2 shows spatial configurations of the reactants and transitions states. Tables 1, 3, and 4 specify optimized geometries, complete energies, and vibrational spectra (for hydrocarbon rádicals only the energies are specified). Figure 5 shows the energetic diagrams of the processes and the differences between the enthalpies $\Delta H_0(0\ K)$ relative to the $F_2Si(C_2H_5)(O–O^{\cdot})$ and $CH_3CH_2CH_2O–O^{\cdot}$ radicals.

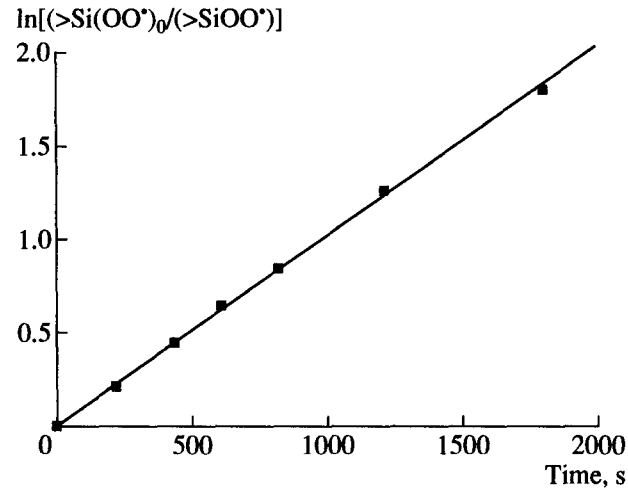

Fig. 4. Kinetics of radical $(\equiv Si–O)_2Si(C_2H_5)(O–O^{\cdot})$ decay at 296 K.

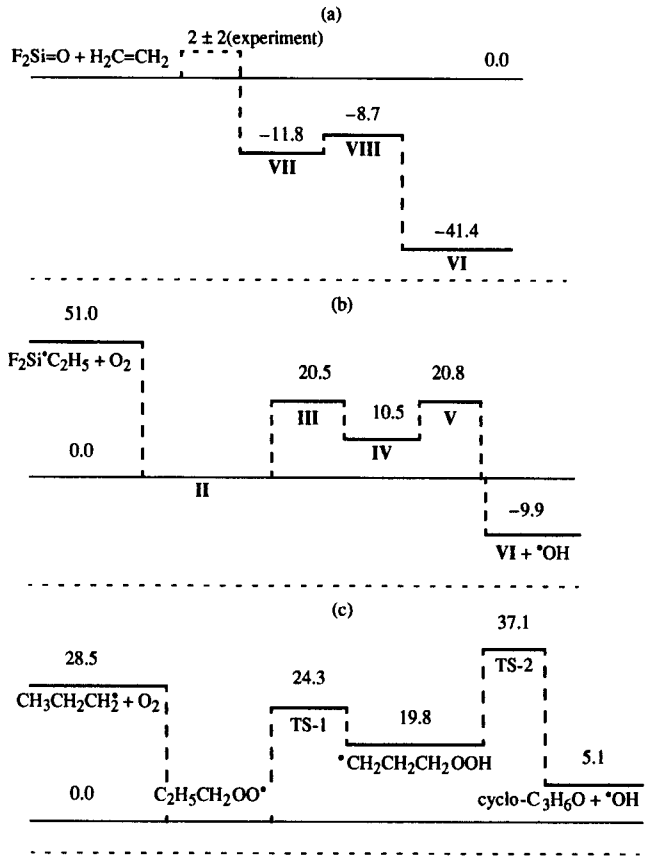

Fig. 5. Energy diagrams of the processes: (a) $F_2Si{=}O + H_2C{=}CH_2$, (b) $F_2Si^{\bullet}C_2H_5 + O_2$, and (c) $CH_3CH_2CH_2^{\bullet} + O_2$. Numbers on the diagram are the enthalpies of the structures (ΔH_0 at 0 K in kcal/mol, DFT calculation) relative to (a) the level of free molecules; (b) $F_2Si(C_2H_5)(O{-}O^{\bullet})$, and (c) $H_3C{-}CH_2CH_2{-}O{-}O^{\bullet}$.

We also calculated the heat of ethyl radical addition to the silylene center $F_2Si{:}$ (–33.3 kcal/mol), which agrees with the experimental fact that radicals **A** are thermally stable below 450 K. The heat of the reaction of oxygen addition to this radical to form a peroxy radical (–51 kcal/mol) is much higher than in the case of a carbon-containing radical (–28.5 kcal/mol). The experimental heat of this reaction in the case of a carbon-containing radical is –30 ± 2 kcal/mol [26].

Figure 2 shows the transition state (**III**) of hydrogen atom transfer from a hydrocarbon fragment to oxygen. The transition state for the transfer of a hydrogen atom in the hydrocarbon radical has a similar structure. The arrows show the directions of atomic shifts as the system moves along the reaction coordinate. It can be seen that the hydrogen atom plays the most important role in this movement. The arrangement of O···H···C atoms in the six-membered transition state is not linear (∠OHC = 156.7°). This points to the internal strains in the cyclic structure. A relatively high value of the activation energy calculated for this reaction is further evidence for that. According to the experimental data [27], the activation energies of hydrogen atom abstraction by the $\equiv Si{-}O{-}O^{\bullet}$ radical from ethane and methane molecules are 8 and 12.5 kcal/mol, respectively. The activation energy of hydrogen atom transfer calculated for the hydrocarbon radical (24.3 kcal/mol) can be compared to a value of 28 kcal/mol reported in [25] for the reaction $(CH_3)_3CCH_2OO^{\bullet} \longrightarrow (CH_3)_2C(CH_2OOH)CH_2^{\bullet}$.

We also calculated the transition states for the hydrogen atom abstraction from the CH_2 group of radicals (a five-membered transition state). As expected, the corresponding transition states are higher (by 6.9 and 8.9 kcal/mol for silicon- and carbon-containing radicals, respectively). Despite the more favorable thermochemistry of the process, the activation energy increases because of the energy of the strain in the transitions state.

According to the literature data, the reaction heat of intramolecular hydrogen transfer from the methyl group to form a hydroperoxy group in the hydrocarbon radical is 10–12 kcal/mol [26, 28]. Thus, the calculation overestimates the reaction heat. To introduce an empirical correction, we calculated at the same level the heats for hydrogen atom abstraction from the HOOH and C_2H_6 molecules. These are 79.7 and 97.3 kcal/mol, respectively. The experimental values are 89 [26] and 100.4 kcal/mol [28]. That is, our calculations underestimated the strength of the O–H bond in hydroperoxide. As a result, the calculated energies for silicon- and carbon-containing hydroperoxides are probably overestimated by ~7 kcal/mol. However, the calculations correctly reflect the trend of increasing O–H bond strength in silicon-containing hydroperoxides. There are no experimental data on the strengths of O–H bonds in hydroperoxide groups connected to a silicon atom. However, analysis of the kinetic data suggests that the O–H bond is stronger in these compounds than in their organic analogs [27]. Therefore, we may assume that the heat of hydrogen atom transfer in the radical **B** is 3–5 kcal/mol. If we assume that the strength of the C–H bond in methyl group of the ethyl fragment is 100 kcal/mol, we obtain the strength of the O–H bond in the Si–O–O–H group (95–97 kcal/mol). This value is much higher than in the hydrogen peroxide molecule and organic hydroperoxides.

Figure 2 shows the structure of the transition state (**V**) for the reaction with the formation of a hydroxyl radical. The arrows point to the directions of atomic shifts as the system moves along the reaction coordinate. The transition state for the hydroxyl abstraction from a hydrocarbon radical has a similar structure, but the activation barrier height is much higher in this case. According to the calculation, the energy of the transition state is even higher than the energy of the $(CH_3CH_2CH_2^{\bullet} + O_2)$ system in the nonbound state. However, the activation energy for the formation of the hydroxyl radical from the alkylhydroperoxide radical

(17.3 kcal/mol, Fig. 5) agrees with an estimate based on experimental kinetic and thermochemical data for the activation energy of oxetane and hydroxyl radical formation by the decomposition of the alkylhydroperoxide radical $(CH_3)_2C(CH_2OOH)CH_2^{\cdot} \longrightarrow$ cyclo-$(CH_3)_2CCH_2OCH_2 + {}^{\cdot}OH$, which is 17 ± 2 kcal/mol [25]. This fact suggests that our calculations overestimated the energies of the hydroperoxide structure and the transition state in the reaction of hydroxyl radical abstraction by ~10 kcal/mol.

Thus, the energies of two transition states for the reactions of hydrogen-atom transfer and hydroxyl radical abstraction from the carbon-containing radical are very close in their values. In the case of a silicon-containing radical, the rate-limiting step of the overall process is the reaction of the intramolecular transfer of a hydrogen atom. The calculated activation energy (~20 kcal/mol) suggests that the reaction may occur at a noticeable rate at room temperature.

Let us discuss the "structure" of the rate constant of radical **B** transformation. According to the kinetic scheme of the process, the decay of peroxy radicals follows the first-order rate law. This agrees with the experimental data (Fig. 4). The apparent rate constant is

$$k_{app} = (k_1k_2)/(k_1 + k_2).$$

Although we hypothesized the rate-limiting step for this process, let us discuss two variants. If $k_{-1} \gg k_2$, then $k_{app} \cong (k_1/k_{-1})k_2$ and the rate-limiting step of the process is hydroxyl radical abstraction. According to transition state theory, $k_{app} = (kT/h)\exp(\Delta S_1/R) \times \exp(-\Delta H_1/RT)$, where ΔS_1 is the difference between the entropies of the transition state for OH radical abstraction and radical **B** and ΔH_1 is the difference of their enthalpy. To estimate the value of the preexponential factor in the rate constant of the reaction (ΔS_1), we used the results of quantum chemical calculations. The difference in the vibrational entropies of **II** and **V** at room temperature is 21.9 – 25.4 = –3.5 cal K^{-1} mol^{-1} (for the radicals grafted to the solid surface translation and rotational degrees of freedom are absent). At 296 K, $(kT/h)\exp(\Delta S_1/R) = 1.0 \times 10^{12}$ s^{-1}. The experimental value of the rate constant $k_{app}(296\ K) = (1 \pm 0.1) \times 10^{-3}$ s^{-1}. Therefore, ΔH_1 = 20.3 kcal/mol. The value of the heat of peroxy radical transformation into hydrocarbon radicals is 3–5 kcal/mol (see above). Then, the activation energy of reaction (VIII) is 15–17 kcal/mol.

In the extreme case when $k_{-1} \ll k_2$, $k_{eff} \cong k_1$, and ΔS_2 = 19.9–25.4 = –5.5 cal K^{-1} mol^{-1} (the difference between the entropies of the peroxy radical and the transition state of hydrogen atom transfer), $(kT/h)\exp(\Delta S_2/R) = 3.9 \times 10^{11}$ s^{-1}. The estimated experimental activation energy for the intramolecular transfer of hydrogen in radical **B** is 19.7 kcal/mol, which agrees with the calculated value for the activation barrier of hydrogen atom transfer in the silicon-containing radical.

The thermal decomposition of the $(\equiv Si–O)_2Si(C_2H_5)(O–O^{\cdot})$ radical can be considered as a convenient heterogeneous reaction for the generation of hydroxy radicals under mild conditions. The possibility for the formation of low-molecular radicals on a "wall," which is usually the surface of a quartz vessel, has been discussed in the literature since the start of chain reaction studies. Our experimental data show the mechanism of this process with concrete surface sites.

CONCLUSION

(1) We developed the method for the synthesis of the $(\equiv Si–O)_2Si(C_2H_5)(O–O^{\cdot})$ radicals grafted on the silica surface and determined the mechanism for their thermal decomposition to form the hydroxy radical and silaoxacyclobutane group. We determined the rate constant for this reaction. It is more facile for silicon-containing peroxy radicals than for carbon-containing radicals.

(2) IR spectral bands were registered for the radicals $(\equiv Si–O)_2Si^{\cdot}–C_2H_5$, $(\equiv Si–O)_2Si(C_2H_5)(O–O^{\cdot})$, and $(\equiv Si–O)_2Si^{\cdot}–OH$.

(3) The mechanism of the interaction of surface silanone groups with molecules was determined. The reaction is accompanied by the formation of silaoxacyclobutane group.

ACKNOWLEDGMENTS

This work was supported by the Russian Foundation for Basic Research (grant no. 97-03-32384) and the Federal Block Program *Environmentally Clean and Resource-Saving Processes in Chemistry and Chemical Engineering* (The Fundamental Problems of Modern Chemistry Subprogram). Quantum chemical calculations were carried out using Gaussuan 94 [7] at the Zelinskii Institute of Organic Chemistry, Russian Academy of Sciences, within the framework of grant no. 98-07-90290 from the Russian Foundation for Basic Research.

REFERENCES

1. Radtsig, V.A., *Kinet. Katal.*, 1983, vol. 24, no. 1, p. 170.
2. Bobyshev, A.A. and Radtsig, V.A., *Khim. Fiz.*, 1988, vol. 7, no. 7, p. 950.
3. Radtsig, V.A. and Kostritsa, S.N., *Izv. Akad. Nauk, Ser. Khim.*, 1997, no. 8, p. 1468.
4. Radtsig, V.A., *Khim. Fiz.*, 1991, vol. 10, no. 9, p. 1262.
5. Morterra, C. and Low, M.J.D., *Ann. N. Y. Acad. Sci.*, 1973, vol. 220, p. 133.
6. Ustynyuk, L.Yu., Radtsig, V.A., and Senchenya, I.N., *Izv. Akad. Nauk, Ser. Khim.*, 1995, no. 12, p. 2409.
7. Frisch, M.J., Trucks, G.W., Schlegel, H.B., *et al.*, *Gaussian 94, Revision D. 1*, Pittsburgh: Gaussian, 1995.
8. Radtsig, V.A., *Kinet. Katal.*, 1996, vol. 37, no. 2, p. 291.

9. Becke, A.D., *J. Chem. Phys.*, 1993, vol. 98, p. 5648.
10. Lee, C., Yang, W., and Parr, R.G., *Phys. Rev. B*, 1988, vol. 37, no. 2, p. 785.
11. Radzig, V.A., *Colloids Surf., A*, 1993, vol. 74, p. 91.
12. Radtsig, V.A., *Kinet. Katal.*, 1979, vol. 20, no. 2, p. 456.
13. Bobyshev, A.A. and Radtsig, V.A., *Kinet. Katal.*, 1990, vol. 31, no. 4, p. 925.
14. Radtsig, V.A., *Kinet. Katal.*, 1996, vol. 37, no. 2, p. 302.
15. Barone, V., Adamo, C., and Russo, N., *Int. J. Quantum Chem.*, 1994, vol. 52, p. 963.
16. Radtsig, V.A., Baskir, E.G., and Korolev, V.A., *Kinet. Katal.*, 1995, vol. 36, no. 4, p. 618.
17. Sverdlov, L.M., Kovner, M.A., and Krainov, E.P., *Kolebatel'nye spektry mnogoatomnykh molekul* (Vibrational Spectra of Polyatomic Molecules), Moscow: Nauka, 1971.
18. Little, L., Infrared Spectra of Adsorbed Species, New York: Academic, 1969.
19. Radtsig, V.A. and Bystrikov, A.V., *Kinet. Katal.*, 1978, vol. 19, no. 3, p. 713.
20. Bobyshev, A.A. and Radtsig, V.A., *Kinet. Katal.*, 1988, vol. 29, no. 3, p. 638.
21. Radtsig, V.A., *Khim. Fiz.*, 2000, vol. 19, no. 3, p. 17.
22. Radtsig, V.A., Berestetskaya, I.V., and Kostritsa, S.N., *Kinet. Katal.*, 1998, vol. 39, no. 6, p. 940.
23. Radtsig, V.A., Berestetskaya, I.V., and Kolbanev, I.V., *Kinet. Katal.* (in press).
24. Ueda, T. and Shimanouchi, K., *J. Chem. Phys.*, 1967, vol. 47, no. 12, p. 5018.
25. Boldwin, R.R., Hisham, M.W.M., and Walker, R.W., *J. Chem. Soc., Faraday Trans. 1*, 1982, vol. 78, p. 1615.
26. Gurvich, L.V., Karachentsev, G.V., Kondrat'ev, V.N., *et al.*, *Energiya razryva khimicheskikh svyazei: Potentsialy ionizatsii i srodstvo k elektronu* (The Energy of Dissociation of Chemical Bonds: Ionization Potentials and Electron Affinity), Moscow: Nauka, 1974.
27. Bobyshev, A.A. and Radtsig, V.A., *Kinet. Katal.*, 1990, vol. 31, no. 4, p. 931.
28. Benson, S.W., *J. Phys. Chem.*, 1996, vol. 100, no. 32, p. 13 544.